

# Theory of electronic and optical properties of bulk AlSb and InAs and InAs/AlSb superlattices

G. Theodorou\* and G. Tsegas

*Department of Physics, Aristotle University of Thessaloniki, 540 06 Thessaloniki, Greece*

(Received 1 September 1999; revised manuscript received 10 December 1999)

An empirical tight-binding model with an orthogonal  $sp^3$  set of orbitals, interactions up to second neighbor, and spin-orbit coupling is used to describe the electronic and optical properties of bulk InAs and AlSb as well as InAs/AlSb superlattices. The tight-binding parameters required for the model are obtained by fitting existing band structures for bulk materials. It is found that with the evaluated tight-binding parameters the model describes very accurately the band structure and the optical properties of the bulk materials. Then the model is used in order to investigate the electronic and optical properties of InAs/AlSb superlattices. It is shown that interface states located in the InSb-like interface quantum wells produce a narrow upper valence band. The effective masses and the variation of the energy gap with interface structure and lattice periodicity are also examined. Additionally the optical functions for the superlattice are calculated, and from the second derivative of  $\epsilon_2$  the critical points are obtained. Finally the optical anisotropy in the superlattice plane is investigated.

## I. INTRODUCTION

In recent years heterostructure systems based on anti-monide compounds and alloys have emerged as some of the most promising compounds for optical device applications. A particular system that has been the subject of considerable attention is that of InAs/AlSb superlattice (SL) structures because of their interesting physical properties as well as their technological importance.<sup>1-11</sup> The very large conduction-band offset<sup>2</sup> of 1.35 eV between InAs and AlSb, and the high electron mobility ( $8 \times 10^5$  cm<sup>2</sup>/V s at 4.2 K) in InAs, make the materials potential candidates for use in the formation of key parts of high-speed electronic devices.<sup>12-14</sup>

The change of both the anion and cation across an InAs/AlSb interface (IF) is a characteristic that makes the former interface different than that for GaAs/(Al, Ga)As and (Ga,In)As/(Al,In)As. As a result, in the InAs/AlSb heterostructure, it is possible to obtain two different types of interfaces.<sup>3</sup> An InSb-like interface, where the InAs layer terminates on an In monolayer and the adjoining AlSb layer starts with an Sb monolayer; and an AlAs-like interface, where the InAs layer terminates on an As monolayer and an Al monolayer immediately after that. In practice, InAs/AlSb SL's can be constructed consisting either of only one of the previously mentioned interface types, or with alternating InSb/AlAs interfaces. Ideal SL's, with sharp interfaces and only one type of interface possess tetragonal symmetry, while SL's with alternating InSb/AlAs interfaces possess orthorhombic symmetry.<sup>9</sup> In the former case, SL's should be isotropic in the layer plane, while in the latter case they will exhibit an optical anisotropy in the superlattice plane. Experiments performed on InAs/AlSb SL's, with the use of spectroscopic ellipsometry and by reflection difference spectroscopy,<sup>9</sup> have revealed the existence of an optical anisotropy not only in structures with alternating AlAs/InSb interfaces but also in those with only InSb or AlAs interfaces. It has been proposed<sup>10</sup> that an intermixing of the atoms across the interface is responsible for the observed anisotropy changes. However, the picture is not clear as yet, especially for the case of SL's with only InSb interfaces; further investigations, both theoretical and experimental, are needed.

The existence of localized interface states in InAs/AlSb SL's, connected to InSb-like interface quantum wells, was first proposed by Kroemer *et al.*,<sup>15</sup> in response to a series of experimental studies<sup>3</sup> related to the observation of a significant excess of electron concentration. Subsequent studies suggested that even though such states may indeed exist, it is not certain that are in fact the source of the carriers.<sup>16-18</sup> Also, *ab initio* pseudopotential calculations demonstrated the existence of such interface-induced localized states in a number of InAs/AlSb SL's.<sup>19,20</sup> We investigate for the presence of such states, and examine their influence on electronic and optical properties of the material.

In this work we present a theoretical investigation of the electronic and optical properties of ideal InAs/AlSb SL's. The calculations are based on an empirical tight-binding (ETB) method, with an  $sp^3$  set of orbitals in the three-center representation. The ETB model was used in the past to describe the III-V compounds with either an  $sp^3s^*$  set of orbitals and nearest-neighbor interactions,<sup>21-23</sup> or with an  $sp^3$  set of orbitals and interactions up to the second-nearest neighbor.<sup>24</sup> The emphasis in those calculations was on describing well the valence bands and energy gaps. This, however, is not sufficient for a description of the optical properties of the materials. To achieve this we must be able to describe accurately the conduction bands as well. In the present work particular effort has been devoted to describing both the valence and conduction bands well. To establish the accuracy of the method, and to obtain the necessary tight-binding parameters, the electronic and optical properties of the bulk materials InAs and AlSb were studied first. The obtained results compare very well with experiment. Then the SL properties were investigated. In particular, the band structure was obtained, and its dependence on the interface structure was examined. A narrow valence band was revealed, produced by the localized states at the InSb-like interface quantum wells. Also, the effective masses for the upper valence and lower conduction bands were calculated, and a variation produced by the various interfaces was found. Additionally the optical functions were calculated for various SL's, and their critical points were uncovered and compared with the experimental results. Finally we have investigated the optical anisotropy in the layer plane for ideal SL's.

TABLE I. Values for the tight-binding model interaction parameters (in eV) of InAs and AlSb, including the spin-orbit coupling constants,  $\lambda_{so}$ . The notation of Slater and Koster is used.

	InAs	AlSb		InAs	AlSb
$E_{ss}^c$	-0.4031	-0.2255	$E_{ss}^c(0.5,0.5,0.0)$	-0.011029	0.156385
$E_{pp}^c$	2.9174	2.2617	$E_{sx}^c(0.0,0.5,0.5)$	-0.062396	-0.159544
$E_{ss}^a$	-8.9133	-7.8290	$E_{sx}^c(0.5,0.5,0.0)$	0.043573	-0.027257
$E_{pp}^a$	0.5597	1.0440	$E_{xx}^c(0.5,0.5,0.0)$	0.313299	0.196373
$E_{ss}(0.25,0.25,0.25)$	-0.822428	-0.717704	$E_{xx}^c(0.0,0.5,0.5)$	-0.183525	-0.194711
$E_{sx}(0.25,0.25,0.25)$	1.182663	1.028487	$E_{xy}^c(0.5,0.5,0.0)$	0.248578	0.191088
$E_{xs}(0.25,0.25,0.25)$	-1.077662	-1.057460	$E_{xy}^c(0.0,0.5,0.5)$	-0.114664	-0.030883
$E_{xx}(0.25,0.25,0.25)$	0.168504	0.135002	$E_{ss}^a(0.5,0.5,0.0)$	-0.225538	-0.207004
$E_{xy}(0.25,0.25,0.25)$	1.399101	1.311837	$E_{sx}^a(0.0,0.5,0.5)$	-0.454499	-0.482288
$\lambda_{so}^c$	0.1290	0.0080	$E_{sx}^a(0.5,0.5,0.0)$	-0.290068	-0.309544
$\lambda_{so}^a$	0.1390	0.3200	$E_{xx}^a(0.5,0.5,0.0)$	0.201376	0.114560
			$E_{xx}^a(0.0,0.5,0.5)$	-0.553861	-0.546311
			$E_{xy}^a(0.5,0.5,0.0)$	0.032127	-0.021574
			$E_{xy}^a(0.0,0.5,0.5)$	-0.432608	-0.313940

## II. METHOD

As stated in Sec. I, the calculations are based on an ETB model Hamiltonian, with an orthogonal  $sp^3$  set of orbitals, interactions up to second-neighbor, and a three-center representation.<sup>25</sup> The spin-orbit interaction is also included in the calculations. The values of the interaction parameters are determined by fitting existing band-structure results with our ETB model. For that purpose the band-structure results of Huang and Ching<sup>26</sup> for AlSb and that of Chelikowsky and Cohen<sup>27</sup> for InAs, are used. The obtained values for the ETB interaction parameters are listed in Table I. From Table I we see that the maximum absolute value for the nearest-neighbor interactions is about 1.5 eV for both materials, while that for the second-neighbor interactions about 0.5 eV, giving a ratio of about 3. The corresponding ratio for the tight-binding parameters of Ref. 24 is about 5.

For the calculation of the imaginary part  $\varepsilon_2(\omega)$  of the dielectric function, the formula<sup>28</sup>

$$\varepsilon_2(\omega) = \frac{4\pi^2 e^2}{m^2 \omega^2} \sum_{c,v} \int \frac{2}{(2\pi)^3} |\langle \mathbf{k}, c | \mathbf{P} \cdot \mathbf{a} | \mathbf{k}, v \rangle|^2 \times \delta[E_{cv}(\mathbf{k}) - \hbar\omega] d\mathbf{k} \quad (1)$$

is used, where  $|\mathbf{k}, c\rangle$  and  $|\mathbf{k}, v\rangle$  stand for the wave functions of the conduction and valence bands, respectively, and  $E_{cv}(\mathbf{k})$  is the energy difference between the  $c$  conduction band and the  $v$  valence band.  $\mathbf{P}$  is the momentum operator, and  $\mathbf{a}$  the polarization unit vector. In our ETB scheme the momentum matrix elements are expressed in terms of the Hamiltonian matrix elements, and distances between localized orbitals.<sup>29-31</sup> The integration in the Brillouin zone (BZ) has been performed within a linear analytic tetrahedron method,<sup>32,33</sup> and for the bulk materials a uniform mesh of  $40 \times 40 \times 40$   $\mathbf{k}$  points has been used. The real part of the dielectric function is obtained by use of the Kramers-Kronig relations.

The model described above is also used for an investigation of the electronic and optical properties of strained materials. A lattice deformation results in a change in the dis-

tances between the atoms and, depending on the type of deformation, a modification of the bond angles. The determination of the new atomic positions of the strained material is a difficult problem. We will approach this problem by using the theory of elasticity. For a calculation of the electronic and optical properties of the strained material, a modification of the Hamiltonian matrix elements is needed in order to incorporate the change in the atomic distances. This is achieved with the use of the scaling formula<sup>25,31</sup>

$$H_{\alpha,\beta}(d) = H_{\alpha,\beta}(d_o)(d_o/d)^{\nu_{\alpha\beta}}, \quad (2)$$

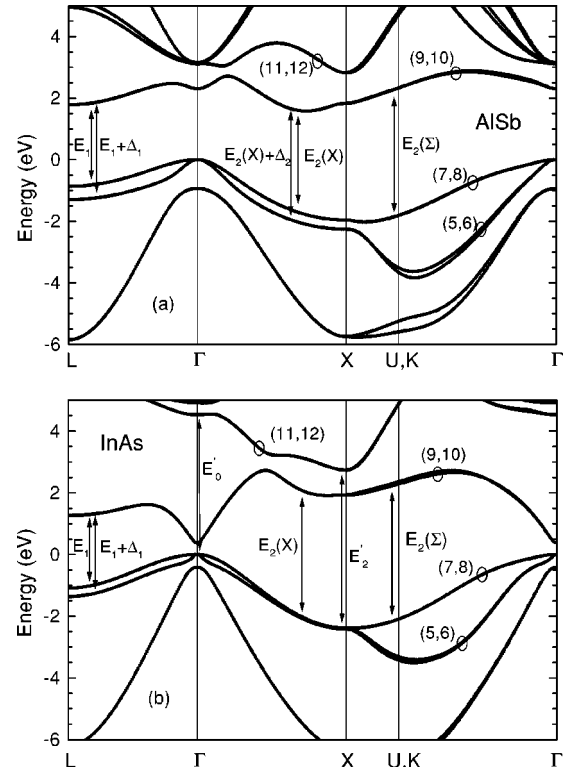


FIG. 1. Calculated band structure for bulk (a) AlSb and (b) InAs. The numbering of the bands, as indicated in the figure, is from the lowest valence band upwards.

TABLE II. Calculated and experimental values for the direct and indirect gaps (in eV) of AlSb and InAs.

		Theory	Experiment <sup>a</sup>
AlSb	$E_g^{dir}(\Gamma_{15v} - \Gamma_{1c})$	2.30	2.38 (25 K), 2.30 (R.T.)
	$E_g^{ind}(\Gamma_{15v} - \Delta_{1c})$	1.57	1.69 (27 K), 1.62 (R.T.)
InAs	$E_g^{dir}(\Gamma_{15v} - \Gamma_{1c})$	0.37	0.42 (4.2 K), 0.35 (R.T.)

<sup>a</sup>Reference 36.

where  $\alpha$  and  $\beta$  represent atomic orbitals and  $d_o$  and  $d$  unstrained and strained interatomic distances respectively. In addition, uniaxial strain along the [001] direction lifts the degeneracy between  $p_x$ ,  $p_y$ , and  $p_z$  orbitals. This modification is taken into account by the linear formula

$$E_p^{x,y} = E_p - b_p(\epsilon_{\parallel} - \epsilon_{\perp}), \quad E_p^z = E_p + 2b_p(\epsilon_{\parallel} - \epsilon_{\perp}), \quad (3)$$

where  $E_p^{x,y}$  and  $E_p^z$  are the on-site  $p$ -orbital integrals, and  $\epsilon_{\parallel}$  and  $\epsilon_{\perp}$  the strain components parallel and perpendicular to the strain axis. The values of the scaling indices  $\nu_{\alpha,\beta}$  and the orbital splitting parameter  $b_p$  are determined in such a way as to obtain the best values for the  $\Gamma$ -point deformation potentials. The optimal set for the scaling parameters, consistent with previous results for III-V compounds,<sup>34</sup> was found to be  $\nu_{ss}=4$ ,  $\nu_{sp}=2$ , and  $\nu_{pp}=2$ , for both materials, with the internal strain parameter<sup>35</sup>  $\zeta$  taken equal to 1 and the orbital splitting parameter  $b_p$  equal to 0, 2, 0.5, and 0.5 eV for As, In, Sb, and Al ions, respectively.

### III. BULK MATERIALS

#### A. Electronic properties

The calculated band structure for AlSb and InAs, using our ETB model, is shown in Fig. 1. The spin-orbit coupling was taken into account in the calculations. InAs is a direct-gap material, while AlSb an indirect one, with the minimum of the conduction band along the  $\Delta$  direction, at the point of  $k=0.73(2\pi/a)$ . The calculated band gaps, together with their experimental values, are shown in Table II. The calculated values come closer to the room-temperature results than to the low temperature experimental results.

The hole and electron effective masses are also calculated for both materials and the resulting values, together with

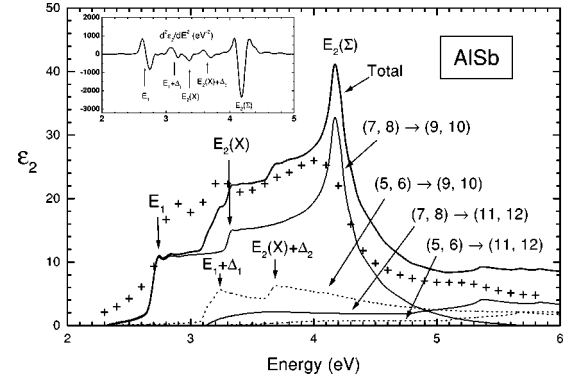


FIG. 2. Calculated imaginary part of the dielectric function,  $\epsilon_2$ , for bulk AlSb. In the figures we also include the experimental data of Ref. 39 for  $\epsilon_2$  (+). In addition, the partial decomposition of  $\epsilon_2$  into contributions from transitions between different valence and conduction bands is also shown. The numbering of the bands is as shown in Fig. 1. Finally, the second derivative of  $\epsilon_2$ ,  $d^2\epsilon_2/d^2E$ , is shown in the inset, with the critical points indicated.

experimental results, are listed in Table III. Our ETB model predicts a large anisotropy between the [001] and [111] directions for the heavy-hole effective masses for both materials. For the case of AlSb, the calculated electron effective masses at the bottom of the conduction band show a large variation between the longitudinal and transverse directions, with the experimental value approximately equal to the mean value of the theoretical ones.

#### B. Optical properties

AlSb: Figure 2 shows the calculated imaginary parts of the dielectric function,  $\epsilon_2$ , for AlSb as a function of energy, together with the experimental data of Zollner *et al.*<sup>39</sup> It is apparent that our ETB model describes the experimental results well; the main difference is in the strength of  $E_2(\Sigma)$  peak, with the theoretical results showing a stronger peak. In the same figure we also show the partial decomposition of  $\epsilon_2$  into contributions from different interband transitions, while as an inset we show the second derivative of  $\epsilon_2$ ; the numbering of the bands starts from the lowest valence band upward, as shown in Fig. 1. The interband transitions from bands (7,8) to (9,10) are responsible for the critical points

TABLE III. Calculated electron and hole effective masses in units of the free-electron mass,  $m_0$ , along with experimental data.

		$m_{hh}^*[100]$	$m_{hh}^*[111]$	$m_{lh}^*[100]$	$m_{lh}^*[111]$	$m_{so}^*$	$m_c^*(\Gamma)$	$m_L^*(\Delta)$	$m_T^*(\Delta)$
InAs	Expt.	0.41 <sup>a</sup>		0.026 <sup>b</sup>		0.024 <sup>b</sup>			
	Theory	0.35 <sup>b</sup>	0.43 <sup>b</sup>						
	Present work	0.426	1.034	0.030	0.029	0.110	0.025		
AlSb	Expt.	0.94 <sup>c</sup>		0.14 <sup>c</sup>		0.39 <sup>a,b</sup>			
	Theory	0.336 <sup>b</sup>	0.872 <sup>b</sup>	0.123 <sup>b</sup>	0.091 <sup>b</sup>				
	Present work	0.304	0.859	0.161	0.120	0.317	0.198	0.560	0.158

<sup>a</sup>Reference 37.

<sup>b</sup>Reference 36.

<sup>c</sup>Reference 38.

TABLE IV. Critical-point energies (in eV) for InAs, AlSb, and the SL  $(\text{InAs})_6/(\text{AlSb})_{6-c}$  grown in a pseudomorphic way on a (001)-AlSb substrate.

$E_S$	$E_1$	$E_1 + \Delta_1$	$E_2(X)$	$E_2(X) + \Delta_2$	$E_2(\Sigma)$	$E'_0$	$E_2$	
InAs								
	2.40	2.66	4.14		4.47	4.76	5.19	Present work
	2.49	2.77			4.5 ( $E'_0$ )	4.7 [ $E_2(X)$ ]		Expt. (Ref. 10)
AlSb								
	2.68	3.15	3.37	3.64	4.18			Present work
	2.81	3.21		3.7 ( $E'_0$ )	4.3			Expt. (Ref. 10)
$(\text{InAs})_6/(\text{AlSb})_{6-c}$								
2.3	2.65	3.0	3.6		4.25			Present work
2.45	2.64	2.88			4.15			Expt. (Ref. 10)

$E_1$ ,  $E_2(X)$ , and  $E_2(\Sigma)$ , resulting from transitions along the  $\Lambda$  direction (close to the  $L$  point), the  $\Delta$  direction (close to the  $X$  point), and the  $\Sigma$  direction (close to the  $K$  point), respectively, while transitions from bands (5,6) to (9,10) are responsible for the critical points  $E_1 + \Delta_1$  and  $E_2(X) + \Delta_2$ . The calculated critical-point energies are given in Table IV, together with the experimental results. The calculated critical points  $E_1 + \Delta_1$  and  $E_2(X)$  are close in energy, and probably will appear as one point in the experiment. The critical point mentioned in Ref. 10 as  $E'_0$  coincides in energy with the calculated  $E_2(X) + \Delta_2$  point. In addition, the partial decomposition of  $\varepsilon_2$  does not show a sharp structure for the  $E'_0$  transitions. Therefore, the  $E'_0$  critical point of Ref. 10 should be reinterpreted as the  $E_2(X) + \Delta_2$  point. With this reinterpretation taken into account, there is an excellent agreement between theory and experiment. The calculated value for the low-frequency dielectric constant is equal to 11.1. For ionic materials, like AlSb, the above calculated quantity corresponds to  $\varepsilon_\infty$ , and is in good agreement with the experimental result<sup>36</sup> equal to 10.24. Finally Fig. 3(a) gives the calculated reflectivity for AlSb, together with the experimental data of Zollner *et al.*<sup>39</sup> The agreement between theory and experiment is excellent.

InAs: Figure 4 shows the calculated imaginary parts of the dielectric function for InAs, as a function of energy, together with the experimental data of Aspnes and Studna.<sup>40</sup> It is apparent from the figure that our ETB model describes the experimental results very well. In the same figure we also show the partial decomposition of  $\varepsilon_2$  into contributions from different interband transitions, while as an inset we show the second derivative of  $\varepsilon_2$ . The interband transitions from bands (7,8) to (9,10) are responsible for critical points  $E_1$  and  $E_2(\Sigma)$ , resulting from transitions along the  $\Lambda$  direction (close to the  $L$  point) and the  $\Sigma$  direction (close to the  $K$  point) respectively. Transitions from bands (5,6) to (9,10) along the  $\Lambda$  direction (close to the  $L$  point) are responsible for the critical point  $E_1 + \Delta_1$ . Transitions from both (7,8) to (9,10) bands and (5,6) to (9,10) bands along the  $\Delta$  direction (close to the  $X$  point) are responsible for the critical point  $E_2(X)$ . Finally, transitions from (7,8) to (11,12) bands near the  $\Gamma$  point are responsible for the critical points  $E'_0$  and  $E'_2$ . The calculated energies for the critical points are given in Table IV, together with the experimental values. The experimental point mentioned as  $E'_0$  coincides in energy with the

calculated  $E_2(\Sigma)$  critical point, and the experimental point mentioned as  $E_2$  coincides with the calculated  $E'_0$ . With this reinterpretation of the experimental data, there is a very good agreement between theory and experiment. The calculated value for the low-frequency dielectric constant is 12.7, and is in good agreement with the experiment result<sup>36</sup> for  $\varepsilon_\infty$ , equal to 12.25. Finally Fig. 3(b) gives the result of our calculations for the reflectivity for InAs, together with the experimental data of Morrison,<sup>41</sup> Philipp and Ehrenreich,<sup>42</sup> and Aspnes and Studna.<sup>40</sup> The agreement between theory and experiment for energies smaller than  $E_2$  is excellent. The main discrepancy at higher energies is with the experimental data of Aspnes and Studna,<sup>40</sup> that show a considerably larger width of the  $E_2$  peak, and which might be the result of the presence of an oxide overlayer on their sample.

#### IV. SUPERLATTICES

Bulk InAs and AlSb compounds crystallize in the zincblende structure with nearly matched lattice constants (with a difference of about 1.25%), that makes the pseudomorphic growth of InAs/AlSb SL's easy. For pseudomorphic growth, the lattice constant in the growth plane is determined by the substrate, while along the growth axis the lattice constant is given to a good accuracy by the elasticity theory. For growth along the [001] direction, the strain in each layer of the con-

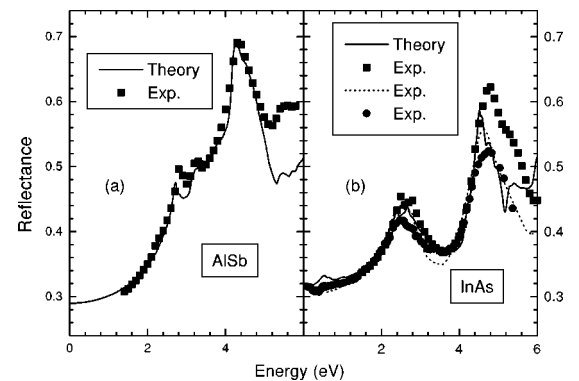


FIG. 3. (a) Calculated reflectivity for bulk AlSb. The experimental data of Ref. 39 (■) are also included. (b) Calculated reflectivity for bulk InAs. The experimental data of Refs. 41, (●), 42 (dotted line), and 40 (■) are also shown.

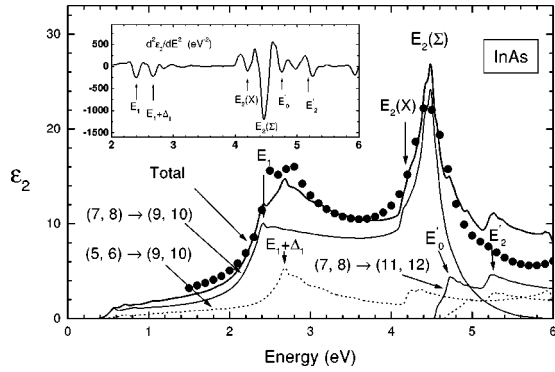


FIG. 4. Calculated imaginary part of the dielectric function,  $\epsilon_2$ , for bulk InAs. In the figure are also included the experimental data of Ref. 40 (●). In addition, the partial decomposition of  $\epsilon_2$  into contributions from transitions between different valence and conduction bands is also shown. The numbering of the bands is as shown in Fig. 1. Finally, the second derivative of  $\epsilon_2$ ,  $d^2\epsilon_2/d^2E$ , is shown in the inset, with the critical points indicated.

stituent material (InAs or AlSb), parallel and perpendicular to the growth plane, will then be given by

$$\epsilon_{\parallel}^i = \frac{a_{\parallel}}{a_i} - 1 \quad (4)$$

and

$$\epsilon_{\perp}^i = \frac{2v_i}{1-v_i} \epsilon_{\parallel}^i, \quad (5)$$

respectively, with  $a_i$  and  $a_{\parallel}$  the lattice constants for the undistorted bulk material and the substrate, respectively, and  $v_i$  the Poisson ratio. Strain modifies the bonds in the constituent materials. In addition, the In-Sb and Al-As bonds at the interfaces were also distorted, and their bond length and bond angles were obtained from elasticity theory applied to the corresponding materials. InAs/AlSb SL's can be constructed either with only InSb IF's, denoted as type-*a* SL's, with only AlAs IF's, denoted as type-*b* SL's; or with alternating InSb, and AlAs IF's, denoted as type-*c* SL's. SL's with an even number of atomic monolayers in the unit cell for each constituent material are of type *c*, e.g.  $(\text{InAs})_6/(\text{AlSb})_{6-c}$ , and possess orthorhombic symmetry<sup>9</sup> ( $C_{2v}$  point-group symmetry), while SL's with an odd number of atomic monolayers for both materials are either of type *a* or *b*, e.g.,  $(\text{InAs})_5\text{In/Sb}(\text{AlSb})_{6-a}$  or  $\text{As}(\text{InAs})_5/(\text{AlSb})_6\text{Al}-b$ , and possess tetragonal symmetry ( $D_{2d}$  point-group symmetry).

### A. Electronic properties

Lattice distortion in the constituent materials in a SL results in a modification of the ETB parameters, that is taken into account as described in Sec. II. Interaction parameters for In-Sb and Al-As bonds at the interface were obtained from the interaction parameters for materials InSb and AlAs, respectively, by appropriate scaling. The values for the tight-binding parameters for these materials are given in the Appendix. The second-neighbor In-Al interactions appearing at some interfaces were approximated by taking the average value between the second-neighbor In-In and second-neighbor Al-Al interactions, scaled at the appropriate dis-

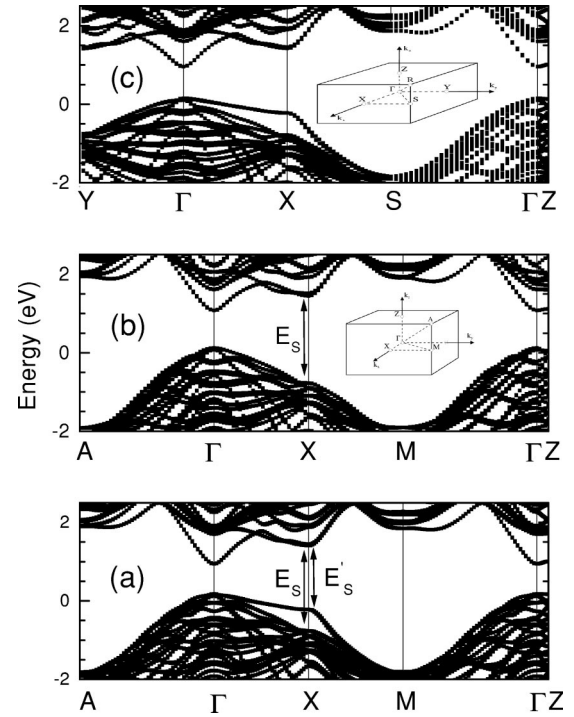


FIG. 5. Calculated band structure for (a)  $(\text{InAs})_5\text{In/Sb}(\text{AlSb})_{6-a}$ , (b)  $\text{As}(\text{InAs})_5/(\text{AlSb})_6\text{Al}-b$ , and (c)  $(\text{InAs})_6/(\text{AlSb})_{6-c}$  SL's, along symmetry lines of the BZ. The inset in (b) shows the BZ structure for a tetragonal structure, and that in (c) the BZ for an orthorhombic structure.

tance. Likewise, the second-neighbor As-Sb interactions were approximated by taking the average value between the second-neighbor As-As and second-neighbor Sb-Sb interactions, scaled at the appropriate distance. In addition, a conduction-band offset between InAs and AlSb equal<sup>2</sup> to 1.35 eV is taken into account, producing a valence-band offset equal to 0.15 eV and a staggered band alignment of bulk materials, and implying that in InAs/AlSb SL's the bottom of the conduction band is an InAs-like band and the top of the valence an AlSb-like band. The band structures for type-*a*, -*b*, and -*c* SL's, namely,  $(\text{InAs})_5\text{In/Sb}(\text{AlSb})_{6-a}$ ,  $\text{As}(\text{InAs})_5/(\text{AlSb})_6\text{Al}-b$ , and  $(\text{InAs})_6/(\text{AlSb})_{6-c}$ , calculated with the present ETB model, are shown in Fig. 5. The above SL's, grown in a pseudomorphic way on an AlSb substrate, are direct-gap materials, having gaps equal to 0.76, 0.96, and 0.80 eV respectively. SL's with orthorhombic symmetry exhibit an anisotropy between the  $\Gamma X$  and  $\Gamma Y$  directions, evident in the band structure of the  $(\text{InAs})_6/(\text{AlSb})_{6-c}$  SL. In addition, the highest valence band in the  $\Gamma X$  direction for type-*a* SL's and in either  $\Gamma X$  or  $\Gamma Y$  directions for type-*c* SL's, is a narrow one. To investigate the nature of the narrow band, the probability amplitudes on the different atoms for the wave function of the previously mentioned narrow valence band for the  $(\text{InAs})_5\text{In/Sb}(\text{AlSb})_{6-a}$  SL were calculated with wave-vector values as indicated in Fig. 6. It is apparent that these states are localized at InSb-like interfaces. In the primitive cell, there exist two InSb-like interface quantum wells for type-*a* SL's, one for type-*c* SL's, and none for type-*b* SL's. For type-*a* SL's, states belonging to the narrow valence band and having wave vectors along the  $[110]$  direction are localized in one of these InSb-like quantum wells, while states with  $\mathbf{k}$  along the  $[\bar{1}10]$  direction are

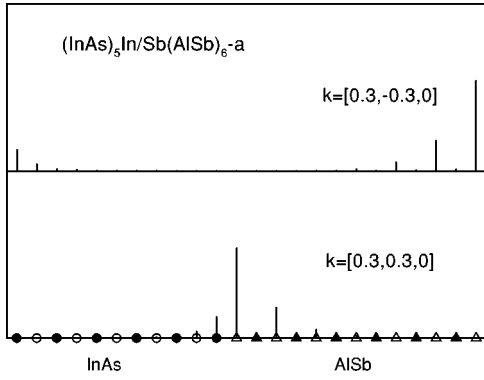


FIG. 6. Probability amplitude (in arbitrary units) on different atomic sites in the unit cell for the upper valence state for the  $(\text{InAs})_5\text{In/Sb(AISb)}_6-a$  SL, with the  $\mathbf{k}$  values as indicated in the figure. Circles denote InAs and triangles AISb sites, with solid symbols denoting cations and hollow anions.

localized in the other, as can be seen from Fig. 6. On the basis of a simple model, this can be understood as follows: In-Sb interface atoms form chains that are directed either along  $[110]$  or  $[\bar{1}10]$  directions, depending on the position of the interface. For type- $c$  SL's, all In-Sb chains are directed along one of the above directions, while for type- $a$  SL's they are directed along both. In the latter case, all chains belonging to equivalent interfaces are directed along the same direction, but chains belonging to neighboring, nonequivalent, interfaces are directed perpendicular to each other. Hopping matrix elements between neighboring In-Sb chains, in the same interface, are weak, because they are mediated through bonds to the InAs and AISb layers, while between neighboring atoms along the chain the hopping matrix elements are strong. As a result, the band produced by the In-Sb interface chains will be a narrow one in the direction perpendicular to the chain axis, and a wide one along it. In particular, chains directed along the  $[\bar{1}10]$  direction will produce a narrow band along the  $[110]$  direction, and a wide one along the  $[\bar{1}10]$  direction, and vice versa. To verify this behavior, the band structure close to the  $\Gamma$  point is calculated for the upper valence bands, and the results are shown in Fig. 7. The lack of inversion symmetry produces the small spin splitting shown in the figure. The  $\text{As(InAs)}_5/(\text{AISb})_6\text{Al}-b$  SL does not possess a narrow valence band; the  $(\text{InAs})_6/(\text{AISb})_6-c$  SL has a narrow valence band along the  $[110]$  direction and a wide one along the  $[\bar{1}10]$  direction; and finally the  $(\text{InAs})_5\text{In/Sb(AISb)}_6-a$  SL, with In-Sb chains in both directions, tends to produce narrow and wide bands in both directions with the net result shown in Fig. 7. States in the wide band will strongly mix with regular valence states and lose their localized character, while in the narrow band the states will remain more or less localized at the interface.

To further investigate the properties of the upper valence bands, their effective masses were calculated and the values given in Table V. These values were obtained by averaging the corresponding values for the spin-split bands. For type- $b$  SL's, with no narrow upper valence band present, the effective mass for the upper valence band is about  $0.26m_0$ . For type- $c$  SL's the effective mass in the direction of the large dispersion (chain axis) is about  $0.13m_0$  and that in the narrow band dispersion (perpendicular to the chain axis) is

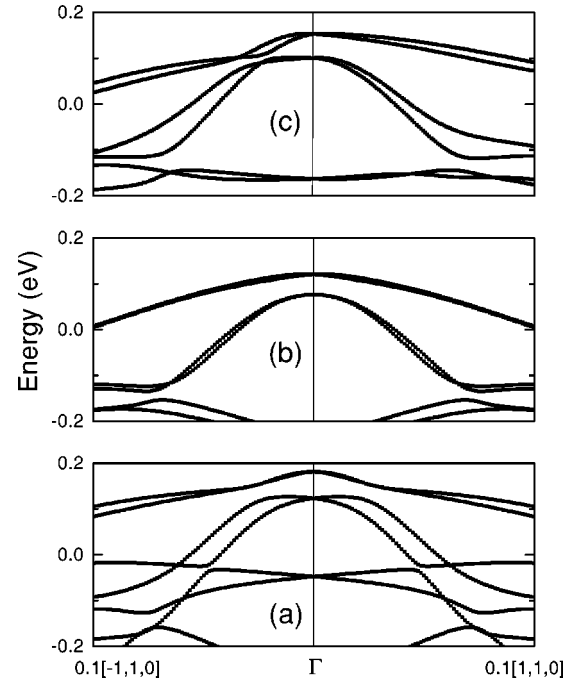


FIG. 7. Band structure, close to the  $\Gamma$  point, for the upper valence bands for (a)  $(\text{InAs})_5\text{In/Sb(AISb)}_6-a$ , (b)  $\text{As(InAs)}_5/(\text{AISb})_6\text{Al}-b$ , and (c)  $(\text{InAs})_6/(\text{AISb})_6-c$  SL's.

about  $0.4m_0$ . Finally for type- $a$  SL's the effective mass is mostly determined by the dispersion of the wide band, and is close to  $0.13m_0$ .

According to the first-principles calculations of Dandrea and Duke,<sup>43</sup> the energy gap for short-period InAs/AISb SL's depends on the interfacial structure, and can be varied by several hundred meV by varying the interface structure. Indeed, an energy difference in the band gaps of about 0.15 eV was experimentally observed<sup>10</sup> for SL's with the same number of atomic layers in the unit cell but with different interface structures, e.g. type- $a$  and - $b$  SL's, with type- $b$  SL's having larger gaps than the corresponding ones for type- $a$  SL's. In order to investigate that effect, the band gaps of  $(\text{InAs})_n\text{In/Sb(AISb)}_{11-n}-a$ ,  $\text{As(InAs)}_n/(\text{AISb})_{11-n}\text{Al}-b$ , and  $(\text{InAs})_n/(\text{AISb})_{12-n}-c$  SL's, grown in a pseudomorphic way on an AISb substrate, were calculated as a function of the number  $m$  of InAs monolayers in the unit cell, equal to  $2n+1$  for type- $a$  and - $b$  SL's and  $2n$  for type- $c$  SL's. The results are shown in Fig. 8. Our calculations show that indeed the energy gap for type- $b$  SL's is larger than that for the corresponding type- $a$  SL's by about 0.2 eV, while type- $c$  SL's have a variation in the middle. This is also in agreement with the theoretical predictions of Dandrea and Duke<sup>43</sup> for a 0.24-eV difference between type- $b$  and - $a$  SL's. In Fig. 8 we also show the experimental results<sup>10</sup> for the energy gaps for  $(\text{InAs})_5\text{In/Sb(AISb)}_6-a$ ,  $\text{As(InAs)}_6/(\text{AISb})_5\text{Al}-b$ , and  $(\text{InAs})_6/(\text{AISb})_6-c$  SL's. There is a good agreement between theory and experiment for first two SL's, while the experimental value for the third one almost lies on a curve corresponding to type- $a$  SL's. This discrepancy might indicate a bad quality of the particular sample.

Finally the band gaps for  $(\text{InAs})_n/(\text{AISb})_n$  SL's, grown in a pseudomorphic way on a AISb substrate, were calculated as a function of the number of InAs monolayers in the

TABLE V. Electron and hole effective masses for several types of InAs/AlSb SL's in units of the free-electron mass  $m_0$ , calculated along the  $[110]$  and  $[1\bar{1}0]$  directions.

Atomic layers	IF's	$m_{v_1}^*[110]$	$m_{v_1}^*[1\bar{1}0]$	$m_{v_2}^*[110]$	$m_{v_2}^*[1\bar{1}0]$	$m_{c_1}^*[110]$	$m_{c_1}^*[1\bar{1}0]$
6/18 (type <i>c</i> )	InSb/AlAs	0.432	0.122	0.133	0.766	0.171	0.189
7/17 (type <i>a</i> )	InSb	0.150	0.150	0.291	0.291	0.160	0.160
7/17 (type <i>b</i> )	AlAs	0.268	0.268	0.159	0.159	0.168	0.168
8/16 (type <i>c</i> )	InSb/AlAs	0.424	0.116	0.128	0.825	0.145	0.162
9/15 (type <i>a</i> )	InSb	0.140	0.140	0.293	0.293	0.128	0.128
9/15 (type <i>b</i> )	AlAs	0.268	0.268	0.150	0.150	0.147	0.147
10/14 (type <i>c</i> )	InSb/AlAs	0.417	0.110	0.122	0.879	0.121	0.132
11/13 (type <i>a</i> )	InSb	0.131	0.131	0.286	0.286	0.105	0.105
11/13 (type <i>b</i> )	AlAs	0.266	0.266	0.140	0.140	0.124	0.124
12/12 (type <i>c</i> )	InSb/AlAs	0.412	0.103	0.115	0.924	0.101	0.109
13/11 (type <i>a</i> )	InSb	0.121	0.121	0.267	0.267	0.086	0.086
13/11 (type <i>b</i> )	AlAs	0.262	0.262	0.129	0.129	0.105	0.105
14/10 (type <i>c</i> )	InSb/AlAs	0.415	0.094	0.106	0.950	0.085	0.090
15/9 (type <i>a</i> )	InSb	0.111	0.111	0.238	0.238	0.071	0.071
15/9 (type <i>b</i> )	AlAs	0.253	0.253	0.117	0.117	0.088	0.088
16/8 (type <i>c</i> )	InSb/AlAs	0.435	0.084	0.095	0.924	0.071	0.074
17/7 (type <i>a</i> )	InSb	0.098	0.098	0.205	0.205	0.057	0.057
17/7 (type <i>b</i> )	AlAs	0.242	0.242	0.103	0.103	0.074	0.074
18/6 (type <i>c</i> )	InSb/AlAs	0.501	0.074	0.081	0.763	0.059	0.060

unit cell, equal to  $m=2n$ , and the results are given as an inset in Fig. 8. The calculated energy gap decreases with  $m$ , indicating carrier confinement into a quantum well. In the limit  $m=\infty$  the quantum wells would possess an infinite width, and the gap would be equal to the energy difference between the bottom of the conduction band for InAs and the top of the valence band for AlSb, equal to 0.22 eV. In the same figure are also included the results obtained by adding, to the minimum gap of 0.22 eV, the increase in energy produced by quantum confinement of the electrons, with an effective mass of  $0.025m_0$ , into a conduction-band quantum

well with a barrier height of 1.35 eV. In this model, tunneling is not taken into account; therefore, the calculated gap will be larger than that for the corresponding superlattice, and will approach the latter for  $m\rightarrow\infty$ . This is indeed the case, as shown in the inset of Fig. 8. Besides electron confinement in the conduction-band quantum well, there is also hole confinement in the valence-band quantum well. Since the valence-band quantum well is quite shallow, 0.15 eV, and the hole effective mass considerably larger than that for electrons, the influence of the valence quantum-well confinement on the band gap will not be significant.

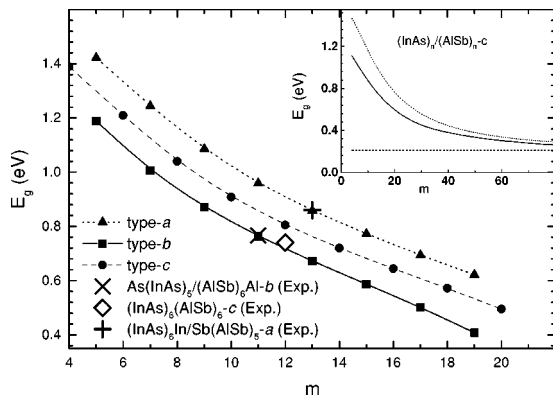


FIG. 8. Band gap for SL's  $(\text{InAs})_n\text{In/Sb}(\text{AlSb})_{11-n-a}$ ,  $\text{As}(\text{InAs})_n/(\text{AlSb})_{11-n}\text{Al}-b$ , and  $(\text{InAs})_n/(\text{AlSb})_{12-n}-c$  as a function of the InAs monolayers,  $m$ , in the primitive cell. In the figure are also shown the experimental results (Ref. 10) for the energy gaps of  $(\text{InAs})_5\text{In/Sb}(\text{AlSb})_6-a$ ,  $\text{As}(\text{InAs})_6/(\text{AlSb})_5\text{Al}-b$ , and  $(\text{InAs})_6/(\text{AlSb})_6-c$  SL's. Finally, the band gap for  $(\text{InAs})_n/(\text{AlSb})_{12-n}-c$  SL's, as a function of the InAs monolayers in the primitive cell,  $m=2n$ , are shown in the inset (solid line). In the inset are also included the results obtained by quantum confinement of electrons in independent wells (dotted line).

## B. Optical properties

Using the present ETB model, the dielectric function for InAs/AlSb SL's has been calculated. The results for the dielectric function, averaged over the three principal axes, are

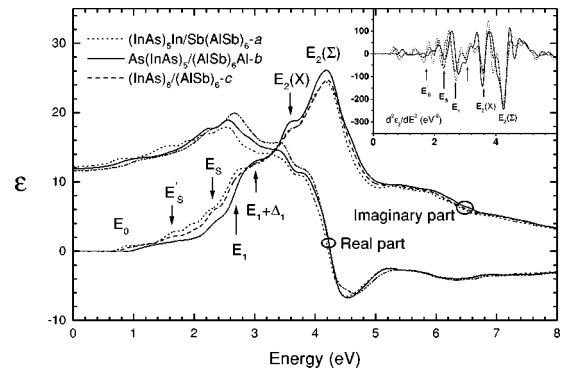


FIG. 9. Real and imaginary parts of the dielectric function for  $(\text{InAs})_5\text{In/Sb}(\text{AlSb})_6-a$ ,  $\text{As}(\text{InAs})_5/(\text{AlSb})_6\text{Al}-b$ , and  $(\text{InAs})_6/(\text{AlSb})_6-c$  SL's. The second derivative of the imaginary part of the dielectric function,  $d^2\epsilon_2/dE^2$ , for the same SL's are shown in the inset, with the critical points indicated.

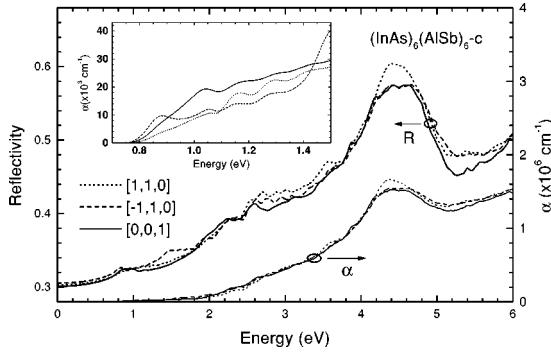


FIG. 10. Reflectivity and absorption coefficient for polarization along three principal axes  $[110]$ ,  $[\bar{1}10]$  and  $[001]$ , for the  $(\text{InAs})_6/(\text{AlSb})_{6-c}$  SL. The inset shows the absorption coefficient near the gap.

shown in Fig. 9 for  $(\text{InAs})_5\text{In/Sb}(\text{AlSb})_{6-a}$ ,  $\text{As}(\text{InAs})_5/(\text{AlSb})_6\text{Al}-b$ , and  $(\text{InAs})_6/(\text{AlSb})_{6-c}$  SL's. The critical points have been obtained from the second derivative of the imaginary part of the dielectric function, shown in the inset of Fig. 9, and their energies for the  $(\text{InAs})_6/(\text{AlSb})_{6-c}$  SL are given in Table IV. In the same table we also include the critical-point energies for the constituent bulk materials, as well as the corresponding average energy for each critical point. The positions of the SL critical points  $E_1$ ,  $E_1 + \Delta_1$ ,  $E_2(X)$ , and  $E_2(\Sigma)$  are near the corresponding average energies for the InAs and AlSb critical points. The experimental energies for  $E_1$  and  $E_1 + \Delta_1$  are equal to<sup>10</sup> 2.65 and 3.0 eV, respectively, in very good agreement to our calculated values of 2.64 and 2.88 eV. Additional critical points  $E_S$  and  $E'_S$ , appear in the SL's, connected to transitions from the valence to conduction bands along the  $\Gamma X$  and/or  $\Gamma Y$  lines, as shown in Fig. 5. The calculated energy for  $E_S$  for  $(\text{InAs})_6/(\text{AlSb})_{6-c}$  SL is 2.3 eV, with the experimental value equal to<sup>10</sup> 2.45 eV. Transitions responsible for the  $E'_S$  critical point are those from the localized valence band to the lowest conduction band. The calculated energy for  $E'_S$  for the  $(\text{InAs})_6/(\text{AlSb})_{6-c}$  SL is 1.65

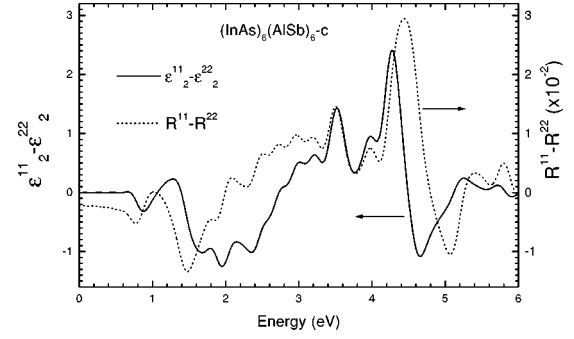


FIG. 11. Anisotropy in  $\epsilon_2$  and reflectivity between directions  $[110]$  and  $[\bar{1}10]$  for the  $(\text{InAs})_6/(\text{AlSb})_{6-c}$  SL.

eV. As can be seen from Fig. 9, the  $E'_S$  critical point is absent in type- $b$  SL's and has its largest strength in type- $a$  SL's. This is because in type- $b$  SL's there is no localized band, in type- $c$  SL's there is a localized band in one direction, and in type- $a$  SL's there are bands in both  $[110]$  and  $[\bar{1}10]$  directions. The calculated strength for the  $E'_S$  structure is small, while the experimental results<sup>10</sup> for the  $(\text{InAs})_6/(\text{AlSb})_{6-c}$  SL do not show such a structure. The absence of an  $E'_S$  structure in the experimental data is probably caused by the intermixing of atoms at the interfaces that destroys the InSb interface quantum wells and the interface states produced by them to a significant extent, or to relaxation effects not included in the present calculations. The calculated zero-frequency dielectric constant, corresponding to  $\epsilon_\infty$ , increases, as expected, with decreasing values of the energy gap, taking values of 11.8, 11.95, and 12.1 for  $\text{As}(\text{InAs})_5/(\text{AlSb})_6\text{Al}-b$ ,  $(\text{InAs})_6/(\text{AlSb})_{6-c}$ , and  $(\text{InAs})_5\text{In/Sb}(\text{AlSb})_{6-a}$  SL's, respectively.

Type- $c$  SL's possess orthorhombic symmetry,<sup>9</sup> with an optical anisotropy in the layer plane. For an investigation of that effect, the reflectivity and absorption coefficients for an  $(\text{InAs})_6/(\text{AlSb})_{6-c}$  SL were calculated for polarizations along the three principal axes  $[110]$ ,  $[\bar{1}10]$ , and  $[001]$ . The results are presented in Fig. 10, showing that the material is

TABLE VI. Values for the tight-binding model interaction parameters (in eV) of AlAs and InSb, including the spin-orbit coupling constants  $\lambda_{so}$ . The notation of Slater and Koster is used.

	AlAs	InSb		AlAs	InSb
$E_{ss}^c$	0.0028	-0.1624	$E_{ss}^c(0.5,0.5,0.0)$	0.160425	-0.070466
$E_{pp}^c$	2.8563	2.0573	$E_{sx}^c(0.0,0.5,0.5)$	-0.200144	0.000358
$E_{ss}^a$	-8.6787	-8.0613	$E_{sx}^c(0.5,0.5,0.0)$	-0.047737	0.084076
$E_{pp}^a$	1.7005	-0.2951	$E_{xx}^c(0.5,0.5,0.0)$	0.220273	0.236072
			$E_{xx}^c(0.0,0.5,0.5)$	-0.119751	-0.125811
$E_{ss}(0.25,0.25,0.25)$	-0.971254	-0.877773	$E_{xy}^c(0.5,0.5,0.0)$	0.176178	0.279387
$E_{sx}(0.25,0.25,0.25)$	1.029127	1.005549	$E_{xy}^c(0.0,0.5,0.5)$	-0.044713	0.233243
$E_{xs}(0.25,0.25,0.25)$	-1.230399	-0.804585	$E_{ss}^a(0.5,0.5,0.0)$	-0.180554	-0.183796
$E_{xx}(0.25,0.25,0.25)$	0.232352	0.032558	$E_{sx}^a(0.0,0.5,0.5)$	-0.422628	-0.373243
$E_{xy}(0.25,0.25,0.25)$	1.465618	1.162185	$E_{sx}^a(0.5,0.5,0.0)$	-0.392094	-0.389780
			$E_{xx}^a(0.5,0.5,0.0)$	0.065390	0.289469
$\lambda_{so}^c$	0.0080	0.1290	$E_{xx}^a(0.0,0.5,0.5)$	-0.538831	-0.580562
$\lambda_{so}^a$	0.1390	0.3200	$E_{xy}^a(0.5,0.5,0.0)$	-0.033664	0.084029
			$E_{xy}^a(0.0,0.5,0.5)$	-0.346760	-0.227121

anisotropic. In addition, the anisotropy between the principal axes  $[110]$  and  $[\bar{1}10]$  is shown in Fig. 11. It has a similar structure in both  $\varepsilon_2$  and the reflectivity, with its strongest values mainly located in the energy region between critical points  $E_0$  and  $E_2$ . Experiments performed on InAs/AlSb SL's with the use of spectroscopic ellipsometry and with reflection difference spectroscopy have revealed the existence of an optical anisotropy in the layer plane not only in type-*c* structures but also in type-*a* and -*b* SL's. The existence of such an anisotropy in type-*a* and -*b* SL's has been attributed to deviations from the ideal superlattice structure produced by interface intermixing of the atoms. However, the picture is not clear as yet, and further investigations, both theoretical and experimental, are needed.

## V. CONCLUSIONS

We have presented an ETB model that describes the electronic and optical properties of InAs and AlSb. The tight-binding parameters required were obtained by fitting existing band structure results with the ETB model (see Table VI). We found that the present model accurately describes not only the band structure of bulk materials but also their optical properties. In particular, the dielectric functions as well as the reflectivity of bulk InAs and AlSb were calculated, and found to be in very good agreement with existing experimental data.

The present ETB model was then used in order to investigate the electronic and optical properties for InAs/AlSb SL's. Their band structure was calculated and the band gaps were obtained. It has been found that for type-*a* and -*b* SL's

the upper valence band is a narrow one, connected to the localized interface states located in the InSb interface quantum wells, while for type-*b* SL's no such band exists. Then the values of the effective masses were calculated, and it was found that the presence of a narrow valence band influences the hole effective masses. It also has been found that the interface structure influences the energy gap. In addition the gap varies with periodicity, and its values have been calculated.

In addition to the band structure, the optical functions for InAs/AlSb SL's were calculated. In particular the real and imaginary parts of the dielectric function were calculated, and the critical points were obtained from the second derivative of  $\varepsilon_2$ . Finally, for an investigation of the anisotropy of the material, the reflectivity and the absorption coefficient were calculated for polarization along the principal axes of the material:  $[110]$ ,  $[\bar{1}10]$ , and  $[001]$ . In particular, the anisotropy in the superlattice plane was investigated, and its values for  $\varepsilon_2$  and the reflectivity are given in Fig. 11.

## APPENDIX

The ETB interaction parameters for AlAs and InSb were obtained by fitting the band-structure results of Huang and Ching<sup>26</sup> for AlAs, and those of Chelikowsky and Cohen<sup>27</sup> for InSb. The obtained values for the ETB interaction parameters are listed in Table VI. The variation of the ETB parameters with strain is described by scaling formula (2), with the optimal values of the exponents found equal to  $\nu_{ss}=4$ ,  $\nu_{sp}=2$ , and  $\nu_{pp}=2$  for both materials, and the internal strain parameter taken equal to 1.

\*Electronic address: theodoru@ccf.auth.gr

- <sup>1</sup>G. Tuttle, H. Kroemer, and J. H. English, *J. Appl. Phys.* **65**, 5239 (1989).
- <sup>2</sup>A. Nakagawa, H. Kroemer, and J. H. English, *Appl. Phys. Lett.* **54**, 1893 (1989).
- <sup>3</sup>G. Tuttle, H. Kroemer, and J. H. English, *J. Appl. Phys.* **67**, 3032 (1990).
- <sup>4</sup>I. Sela, C. R. Bolognesi, L. A. Samoska, and H. Kroemer, *Appl. Phys. Lett.* **60**, 3289 (1992).
- <sup>5</sup>C. R. Bolognesi, H. Kroemer, and J. H. English, *Appl. Phys. Lett.* **61**, 213 (1992).
- <sup>6</sup>J. R. Waldrop, G. J. Sullivan, R. W. Grant, E. A. Kraut, and W. A. Harrison, *J. Vac. Sci. Technol. B* **10**, 1773 (1992).
- <sup>7</sup>J. Spitzer, H. D. Fuchs, P. Etchegoin, M. Ilg, M. Cardona, B. Brar, and H. Kroemer, *Appl. Phys. Lett.* **62**, 2274 (1993).
- <sup>8</sup>B. Brar, J. Ibbetson, H. Kroemer, and J. H. English, *Appl. Phys. Lett.* **64**, 3392 (1994).
- <sup>9</sup>P. V. Santos, P. Etchegoin, M. Cardona, B. Brar, and H. Kroemer, *Phys. Rev. B* **50**, 8746 (1994).
- <sup>10</sup>J. Spitzer, A. Höpner, M. Kuball, M. Cardona, B. Jenichen, H. Neuroth, B. Brar, and H. Kroemer, *J. Appl. Phys.* **77**, 811 (1995).
- <sup>11</sup>D. Toet, B. Koopman, P. V. Santos, R. B. Bergmann, and B. Richards, *Appl. Phys. Lett.* **69**, 3719 (1996).
- <sup>12</sup>G. Tuttle and H. Kroemer, *IEEE Trans. Electron Devices* **ED-34**, 2358 (1987).
- <sup>13</sup>L. F. Luo, R. Beresford, and W. I. Wang, *Appl. Phys. Lett.* **53**, 2320 (1988).

- <sup>14</sup>C. R. Bolognesi, M. W. Dvorak, and D. H. Chow, *J. Vac. Sci. Technol. A* **16**, 843 (1998).
- <sup>15</sup>H. Kroemer, C. Nguyen, and B. Brar, *J. Vac. Sci. Technol. B* **10**, 1769 (1992).
- <sup>16</sup>S. Ideshita, A. Furukawa, Y. Mochizuki, and M. Mizuta, *Appl. Phys. Lett.* **60**, 2549 (1992).
- <sup>17</sup>D. J. Chadi, *Phys. Rev. B* **47**, 13 478 (1993).
- <sup>18</sup>J. Shen, H. Goronkin, J. Dow, and S. Y. Ren, *J. Appl. Phys.* **77**, 1576 (1995).
- <sup>19</sup>M. J. Shaw, P. R. Briddon, and M. Jaros, *Phys. Rev. B* **52**, 16 341 (1995).
- <sup>20</sup>M. J. Shaw, G. Gopit, P. R. Briddon, and M. Jaros, *J. Vac. Sci. Technol. B* **16**, 1794 (1998).
- <sup>21</sup>P. Vogl, H. P. Hjalmarson, and J. D. Dow, *J. Phys. Chem. Solids* **44**, 365 (1983).
- <sup>22</sup>J. N. Schulman and Y.-C. Chang, *Phys. Rev. B* **31**, 2056 (1985).
- <sup>23</sup>C. Priester, G. Allan, and M. Lannoo, *Phys. Rev. B* **37**, 8519 (1988).
- <sup>24</sup>D. N. Talwar and C. S. Ting, *Phys. Rev. B* **25**, 2660 (1982).
- <sup>25</sup>C. Tserbak, H. M. Polatoglou, and G. Theodorou, *Phys. Rev. B* **47**, 7104 (1993).
- <sup>26</sup>M. Huang and W. Y. Ching, *J. Phys. Chem. Solids* **46**, 977 (1985).
- <sup>27</sup>J. R. Chelikowsky and M. L. Cohen, *Phys. Rev. B* **14**, 556 (1976).
- <sup>28</sup>F. Wooten, *Optical Properties of Solids* (Academic Press, New York, 1972).
- <sup>29</sup>N. V. Smith, *Phys. Rev. B* **19**, 5019 (1979).

- <sup>30</sup>L. Brey and C. Tejedor, *Solid State Commun.* **48**, 403 (1983).
- <sup>31</sup>C. Tserbak and G. Theodorou, *Phys. Rev. B* **50**, 18 179 (1994).
- <sup>32</sup>O. Jepsen and O. K. Andersen, *Solid State Commun.* **9**, 1763 (1971).
- <sup>33</sup>G. Lehmann and M. Taut, *Phys. Status Solidi B* **54**, 469 (1972).
- <sup>34</sup>G. Theodorou and G. Tsegas, *Phys. Status Solidi B* **211**, 847 (1999).
- <sup>35</sup>L. Kleinman, *Phys. Rev.* **128**, 2614 (1962).
- <sup>36</sup>*Physics of Group IV Elements and III-V Compounds*, edited by O. Madelung, Landolt-Börnstein, New Series, Group III, Vol. 17, Pt. a (Springer, Berlin 1991).
- <sup>37</sup>D. Long in *Energy Bands in Semiconductors* (Interscience, New York, 1968).
- <sup>38</sup>P. Lawaetz, *Phys. Rev. B* **4**, 3460 (1971).
- <sup>39</sup>S. Zollner, C. Lin, E. Schönherr, A. Böhringer, and M. Cardona, *J. Appl. Phys.* **66**, 383 (1989).
- <sup>40</sup>D. E. Aspnes and A. A. Studna, *Phys. Rev. B* **27**, 985 (1983).
- <sup>41</sup>R. E. Morrison, *Phys. Rev.* **124**, 1314 (1961).
- <sup>42</sup>H. R. Philipp and H. Ehrenreich, *Phys. Rev.* **129**, 1550 (1963).
- <sup>43</sup>R. G. Dandrea and C. B. Duke, *Appl. Phys. Lett.* **63**, 1795 (1993).